Acquisition and tracking for communications between Lunar South Pole and Earth

Dariush Divsalar
Jet Propulsion Laboratory
California Institute of Technology
Pasadena, CA 91109
Dariush.Divsalar@jpl.nasa.gov

Marc Sanchez Net
Jet Propulsion Laboratory
California Institute of Technology
Pasadena, CA 91109
Marc.Sanchez.Net@jpl.nasa.gov

Kar-Ming Cheung
Jet Propulsion Laboratory
California Institute of Technology
Pasadena, CA 91109
Kar-Ming.Cheung@jpl.nasa.gov

Abstract*—In this paper we design and analyze an end-to-end communication system between a lander/rover on the surface of the lunar South Pole and an Earth station. The acquisition and tracking system is discussed in detail. The communication system on the lander or rover could be used for the Earth-to-Moon communication. To communicate to and from the lander/rover on the lunar South Pole, low and/or medium directional antennas onboard the lander/rover will have to be pointed at low elevation angles between 2 to 10 degrees, thus causing multipath fading effects due to reflection of a portion of the transmitted electromagnetic waves from the surface of the Moon that are not commonly encountered in traditional deep space communications between a spacecraft and a ground station. To design and analyze such a communication system, and in particular the acquisition and tracking system, in the presence of multipath fading, first we model the fading channel based on existing and simulated data. In addition to multipath fading, the channel also introduces Doppler frequency up to 11.5 KHz, and Doppler rate up to 0.735 Hz/sec. For coherent reception the Doppler frequency, which is time varying, should be acquired and the incoming carrier phase, which includes the fading phase, should be tracked in the presence of multipath fading. For this communication system in addition to estimating the received carrier phase, the amplitude of the fading signal should also be estimated, in particular to be used in the decoder. In addition to acquisition and tracking, we consider simple modulation and coding schemes. Space diversity using two antennas on earth to mitigate the effects of fading could also be used. We design phase-locked loops and frequency sweeping schemes robust to the attenuations due to fading. After designing various components of the communication system, we use Simulink models to obtain the end-to-end performance of the communication link under investigation. Based on the available data, the fading channel can be accurately modeled as a Rician fading channel with Rician parameter of 10 dB, and Doppler spread that depends on the Doppler frequency and the transmit/receive antenna patterns. The challenge is how to make such a communication system robust in the presence of the multipath fading where the Doppler spread changes in time and thus produces fading with time-varying durations (short and very long fades). In summary, this paper covers communication system design, performance analysis, and simulations for performance of Doppler frequency acquisition, tracking, uncoded system, and coded system under ideal interleaving assumption with hard decision over communication link between a lander/rover at the Lunar south pole and a DSN Earth station in presence of Rician fading.

TABLE OF CONTENTS

1. INTRODUCTION 1
2. SYSTEM MODEL 2
3. FADING CHANNEL MODEL 2
4. PERFORMANCE OF UNCODED BPSK IN PRESENCE OF FADING WITH PHASE ERROR 5
5. FREQUENCY ACQUISITION AND TRACKING USING PLL WITH SMART FREQUENCY SWEEPING 5
6. A SETUP FOR SYSTEM SIMULATION 6
7. CONCLUSIONS 7
ACKNOWLEDGMENTS 7
REFERENCES 8
BIOGRAPHY 8

978-1-5386-6854-2/19/$31.00 ©2019 IEEE

1. INTRODUCTION

There is an interest to map/sample surface volatiles, to explore possible reservoirs of water ice existing in permanently shadowed areas of the lunar South Pole as shown in Fig.1. In this paper we design and analyze an end-to-end communication system between a lander/rover on the surface of the lunar South Pole and an Earth station as shown in Fig.2. There are communication systems on the rover and the lander. One of the communication systems is used for Earth-to-Moon communication. To communicate to and from the lander/rover on the lunar South Pole, low and/or medium directional antennas onboard the lander/rover will have to be pointed at low elevation angles between 2 to 10 degrees, thus causing multipath fading effects due to reflection of a portion of the transmitted electromagnetic waves from the surface of the Moon that are not commonly encountered in traditional deep space communications between a spacecraft and a ground station. To design and analyze such a communication system, and in particular the acquisition and tracking system, in the presence of multipath fading, first we model the fading channel based on existing and simulated data. In addition to multipath fading, the channel also introduces Doppler frequency up to 11.5 KHz, and Doppler rate up to 0.735 Hz/sec. The Doppler frequency profile is shown in Fig.3, and the Doppler frequency rate profile is shown in Fig. 4. For coherent reception the Doppler frequency, which is time-varying, should be acquired, and the incoming carrier phase, which includes the fading phase, should be tracked in the presence of multipath fading. For this communication system, in addition to estimating the received carrier phase, the amplitude of the fading signal should also be estimated, in particular to be used in the decoder. In addition to acquisition and tracking, we consider simple modulation and coding with ideal interleaving (see section 6) schemes. Space diversity using two antennas on earth to mitigate the effects of fading could also be used, but it was not addressed in this paper. We design phase-locked loops and frequency sweeping schemes robust to the attenuations due to fading. After designing various components of the communication system, we use Simulink models to obtain the end-to-end performance of the communication link under investigation. Based on the available data, the fading channel can be accurately modeled as a Rician fading channel with Rician parameter of 10 dB, and Doppler spread that depends on the Doppler frequency

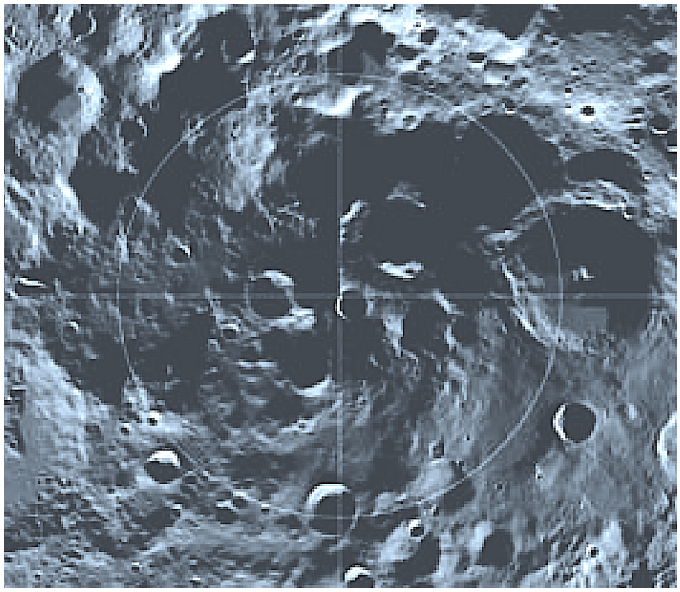

Figure 1. South Pole region of the Moon.

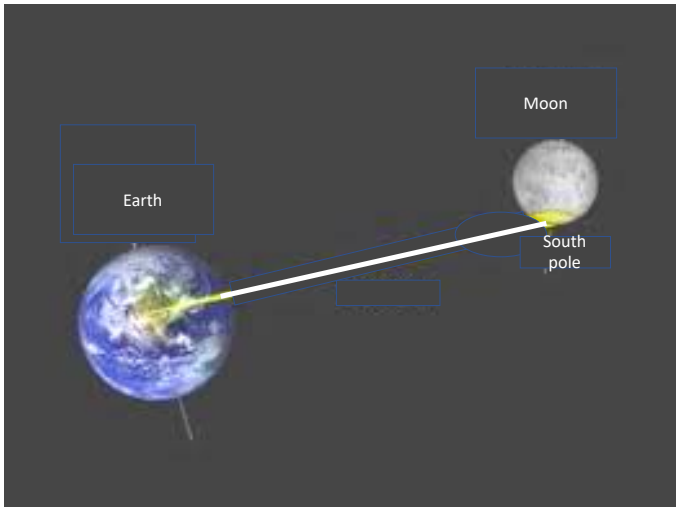

Figure 2. Communication link between the South Pole of the Moon and Earth.

and the transmit/receive antenna patterns. The challenge is how to make such a communication system robust in the presence of the multipath fading, where the Doppler spread changes in time and thus produces fading with time-varying durations (short and very long fades). In summary, the paper covers communication system design, performance analysis, and simulations.

2. System Model

Consider a communication system in which a user is communicating with a binary phase-shift keying (BPSK) data modulation over a fading and additive white Gaussian noise (AWGN) channel. Let P_t be the total received average power, T_s the data symbol time duration, and N_o W/Hz the single-sided power spectral density (PSD) of the AWGN. At baseband, this signal can be written in the complex form

$$y(t) = \sqrt{P_t}F(t)e^{j(2\pi(f_c+\Delta f+rt)t+\beta m(t)g(t)+\theta)} + n(t) \quad (1)$$

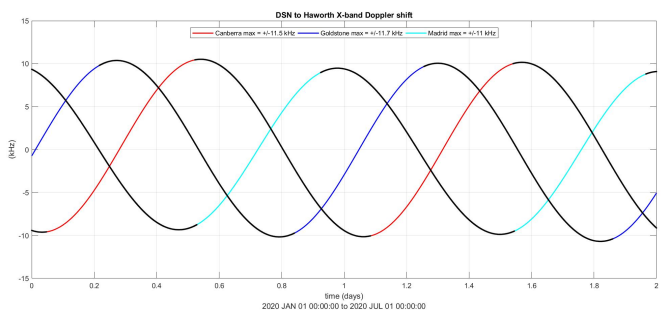

Figure 3. Doppler frequency profile for link between South Pole of the Moon and Earth.

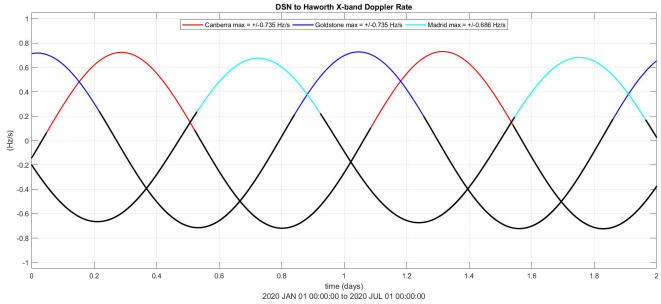

Figure 4. Doppler rate profile for link between South Pole of the Moon and Earth.

where, $m(t) = \sum_{k=-\infty}^{\infty} a_k p(t - kT_s)$ represent the BPSK data modulation, with the k-th bit taking on values $a_k \in \{+1, -1\}$, $p(t)$ is a unit-power rectangular pulse shape of duration T_s , θ is the carrier phase, Δf is Doppler frequency, and r is Doppler rate. The waveform $g(t)$ corresponds to the subcarrier, it can be a sine waveform subcarrier $g(t) = \sin(2\pi f_{sc}t)$, or a square waveform subcarrier $g(t) = \text{Sign}(\sin(2\pi f_{sc}t)) = \text{Sq}(2\pi f_{sc}t)$; if $g(t) = 1$ then there is no subcarrier. The $n(t)$ term is zero-mean complex Gaussian white noise with two-sided power spectral density $N_o/2$. The parameter β represents the modulation index. The multiplicative factor $F(t)$ is a complex fading process. Since it is assumed that a direct line of sight (LoS) exists, the magnitude of $F(t)$ is assumed to be Rician distributed. Its phase contributes to the carrier phase, and the resulting total phase should be tracked for coherent reception of data.

3. Fading Channel Model

As discussed in the Introduction section, to communicate to and from the lander/rover on the lunar South Pole, low and/or medium directional antennas onboard the lander/rover will have to be pointed at low elevation angles between 2 to 10 degrees, thus causing multipath fading effects due to reflection of a portion of the transmitted electromagnetic waves from the surface of the Moon. The power in the reflected wave depends on the reflection coefficient at the soil surface which is related to the dielectric constant of the soil. An RF signal at carrier frequency f_c that is transmitted by the lander/rover to Earth in a typical lunar surface environment may exhibit variations in amplitude, phase, and apparent frequency. The fading effects are due to the random distribution of the electromagnetic field reflecting from the rough lunar surface and its variation is due to relative velocity and velocity rate (range change) of the Moon (lander/rover at

its South Pole) with respect to Earth (DSN antenna). In such a scenario the reflected electromagnetic field can be expressed as a linear superposition of plane waves of random phase. The frequency of each reflected wave is affected by a Doppler frequency shift. This frequency shift is due to relative Earth-Moon velocity, operating carrier frequency, and the angle the propagation vector makes with the velocity vector. The power spectra of the received signal at an Earth station depends on the density of the arrival angles of the reflected plane waves from the lunar surface, and on the antenna directivity patterns at both the South Pole lander/rover and the DSN Earth station. Since the DSN antenna is very high gain, having a very narrow beamwidth and pointing toward the Moon, it is expected that no reflected wave from the surface of Earth will be captured by the DSN antennas. The received faded signal in general can be characterized by three components, the direct line-of-sight (LOS), the specular component, and the diffuse component. The combined direct and specular components are referred to as the coherent received component, and the diffuse component is referred to as the non-coherent received component. The specular component is due to a strong reflection over a very smooth surface. A very smooth surface on the Moon near its South Pole is not expected in this study. Therefore in this paper, it is assumed that there are two main components in the received faded signal, the direct line of sight and the diffuse component. Such a fading model is referred to Rician fading [1], [2], [3], [4], [5], [6] .

The field from the reflected diffuse component as seen by the receiving antenna can be modeled as

$$e(t) = \sum_{i=1}^{N} e_i \cos(2\pi(f_c + f_i)t - \phi_i) \tag{2}$$

where e_i the amplitude of the received i-th wave field, $f_i = \frac{v}{c} f_c \cos\theta_i$ is due to the relative velocity, and θ_i is the angle between the direction of the velocity vector v corresponds to velocity of the Deep Space Network (DSN) with respect to the Lunar south pole. The projection of this velocity vector into a line tangent to the surface of Earth corresponds to the rotation speed of Earth at the DSN, and the i-th incident wave. The maximum of f_i is the Doppler frequency $f_m = \frac{v}{c} f_c$ where c denotes the speed of light. If we have a high gain antenna at the DSN pointed in the direction of the Lunar south pole, this maximum Doppler frequency f_m, might not even be observed by the receiver. The phase ϕ_i is uniformly distributed between 0 and 2π. For large enough N by the central limit theorem the field $e(t)$ is approximately a Gaussian random process. Since the Doppler frequency f_m is much smaller than the carrier frequency f_c, then $e(t)$ is narrow band. This process also can be assumed to be wide-sense stationary, and since it is Gaussian then it is stationary. Thus the random process $e(t)$ can be represented as

$$e(t) = N_I(t)\cos(2\pi f_c t) - N_Q(t)\sin(2\pi f_c t) \tag{3}$$

where $N_I(t)$ and $N_Q(t)$ are narrow-band stationary independent Gaussian processes. The means of these processes are zero and they have the same variance σ_F^2. Let the direct line-of-sight signal be denoted by

$$A\cos(2\pi(f_c + f_d)t)$$

where $f_d = f_m \cos(\eta)$, and η is angle between the antenna velocity vector and the antenna bearing pointed in the direction of line-of-sight toward the Lunar south pole. This signal can be represented as

$$A\cos(2\pi f_d t)\cos(2\pi f_c t) - A\sin(2\pi f_d t)\sin(2\pi f_c t)$$

Thus the overall fading signal can be expressed as

$$\begin{aligned} f(t) &= (A\cos(2\pi f_d t) + N_I(t))\cos(2\pi f_c t) \\ &\quad -(A\sin(2\pi f_d t) + N_Q(t))\sin(2\pi f_c t) \end{aligned} \tag{4}$$

We can define the complex fading signal as

$$F(t) = (A\cos(2\pi f_d t) + N_I(t)) + j(A\sin(2\pi f_d t) + N_Q(t)) \tag{5}$$

Both components are independent Gaussian processes with means μ_I and μ_Q and the same variance σ_F^2. At this point we define the Rician parameter K as

$$K = \frac{\mu_I^2 + \mu_Q^2}{2\sigma_F^2} = \frac{A^2}{2\sigma_F^2} \tag{6}$$

Let the power of the fading be normalized to unity, $E\{|F(t)|^2\} = 1$. Let $\rho(t) = |F(t)|$ be the magnitude of $F(t)$, and let the phase of $F(t)$ be denoted by $\theta(t)$. Then for any fixed time t the probability density function of $\rho(t) = \rho$ is given as [9]

$$p(\rho) = 2(K+1)\rho e^{-(K+1)\rho^2 - K} I_0(2\rho\sqrt{K(K+1)}) \tag{7}$$

and for any fixed time t the probability density function of $\theta(t) = \theta$ is given as

$$p(\theta) = \frac{1}{2\pi} + \frac{1}{2}\sqrt{\frac{K}{\pi}}\cos\theta\, e^{-K\sin^2\theta}\left[1 + erf(\sqrt{K}\cos\theta)\right] \tag{8}$$

where $I_0(\cdot)$ is the zero-order modified Bessel function of the first kind.

As it is mentioned previously, based on the available data, the Rician parameter is K=10 dB. We will shortly discuss the power spectrum of the diffuse fading signal and variations of the received power due to fading. But at this point, assuming perfect tracking of Doppler frequency, carrier phase tracking, and having perfect time synchronization of data, the conditional bit error probability $P_b(\rho)$ of uncoded BPSK modulation in the presence of Rician fading given the amplitude of the fade ρ and assuming the average power of fade is normalized to unity, can be obtained as

$$P_b(\rho) = Q(\sqrt{2\frac{\bar{E}_b}{N_o}}\rho) \tag{9}$$

where $\frac{\bar{E}_b}{N_o}$ is the average received bit signal-to-noise ratio, and

$$Q(x) = \int_{u=x}^{\infty} \frac{1}{\sqrt{2\pi}} e^{-\frac{u^2}{2}}\, du \tag{10}$$

To find the unconditional bit error rate we need to average $P_b(\rho)$ over the probability density of ρ, denoted by $p(\rho)$.

$$P_b = \int_{\rho=0}^{\infty} P_b(\rho)p(\rho)d\rho \tag{11}$$

Using the above equation, the bit error rate performance of BPSK versus the average bit signal-to-noise ratio $\frac{E_b}{N_o}$ is shown in Fig. 5. Note that $Q(x)$ can also be represented as

$$Q(x) = \frac{1}{\pi}\int_{\theta=0}^{\frac{\pi}{2}} e^{-\frac{x^2}{2\sin^2\theta}}\, d\theta \tag{12}$$

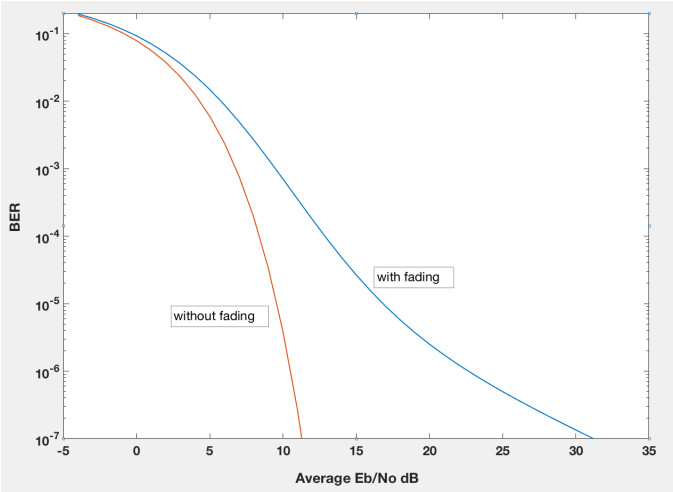

Figure 5. BER vs E_b/N_o for no fading and Rician fading with K=10 dB under perfect time, Doppler, and phase synchronization

A simple upper bound can be obtained by upper bounding $e^{-\frac{x^2}{2\sin^2\theta}} \leq e^{-\frac{x^2}{2}}$ for $0 \leq \theta \leq \frac{\pi}{2}$ to get

$$Q(x) \leq \frac{1}{\pi}\int_{\theta=0}^{\frac{\pi}{2}} e^{-\frac{x^2}{2}}\,d\theta = \frac{1}{2}e^{-\frac{x^2}{2}} \tag{13}$$

Using the upper bound on $Q(x)$ then we can obtain an upper bound on P_b as

$$P_b \leq \frac{1}{2}\frac{K+1}{K+1+\frac{\bar{E}_b}{N_o}} e^{-\frac{K\frac{\bar{E}_b}{N_o}}{K+1+\frac{\bar{E}_b}{N_o}}} \tag{14}$$

When there is no fading and under perfect synchronization then

$$P_b = Q(\sqrt{2\frac{E_b}{N_o}}) \leq \frac{1}{2}e^{-\frac{E_b}{N_o}} \tag{15}$$

If we want to achieve the same bit error rate as in a no-fading case corresponding to an ideal $\frac{E_b}{N_o}$, then we can approximately compute the required $\frac{\bar{E}_b}{N_o}$ by solving the following equation to obtain the degradation due to fading.

$$\frac{K\frac{\bar{E}_b}{N_o}}{K+1+\frac{\bar{E}_b}{N_o}} - \ln\frac{K+1}{K+1+\frac{\bar{E}_b}{N_o}} = \frac{E_b}{N_o} \tag{16}$$

Power Spectrum of Fading Signal

The following is based on Jakes's results [5]. First the Power Spectral Density (PSD) is obtained for the diffuse process, which corresponds to the reflected waves from the Lunar surface near the South Pole. Let the angle between the direction-of-velocity vector and the direction of a typical diffuse wave component arriving at the receiving antenna be γ. The power contribution to the received signal by the diffuse waves arriving from the scattering of rough objects on the lunar surface around the lander/rover within an angle $d\gamma$ is proportional to $p(\gamma)G(\gamma-\eta)d\gamma$ where $p(\gamma)$ is the angular density function of the wave arrival angles, and $G(\gamma-\eta)$ is the antenna gain pattern. Recall that η is angle between the velocity vector and the antenna bearing pointed in the direction of line-of-sight toward the Lunar south pole. If $S(f)$ is the power spectral density of the received diffuse signal, then the power contribution of a Doppler frequency within the range of frequency df is $S(f)|df|$. The Doppler frequency is $f = f_m\cos\gamma$ where $f_m = \frac{v}{c}f_c$ is the maximum Doppler frequency shift. Since the two angles γ and $-\gamma$ can result in the same Doppler frequency, the contribution of power at angles γ and $-\gamma$ within the differential angle $d\gamma$, resulting in the Doppler frequency f, is proportional to $(p(\gamma)G(\gamma-\eta)+p(-\gamma)G(-\gamma-\eta))d\gamma$. Thus $S(f)|df| = \alpha(p(\gamma)G(\gamma-\eta)+p(-\gamma)G(-\gamma-\eta))d\gamma$ where α is a constant. Since $f = f_m\cos\gamma$, then $df = -f_m\sin\gamma\,d\gamma$. But $\sin\gamma = \sqrt{1-\cos^2\gamma}$ or $|df| = f_m\sqrt{1-\frac{f}{f_m}^2}d\gamma$. Therefore

$$S(f) = \frac{\alpha(p(\gamma)G(\gamma-\eta)+p(-\gamma)G(-\gamma-\eta))}{\sqrt{f_m^2-f^2}} \tag{17}$$

If we assume β_b is beamwidth of the receiving antenna then $|\gamma-\eta| \leq \frac{\beta_b}{2}$. So approximately we can assume $p(\gamma)$ is uniformly distributed within this angle and the gain of the antenna is non-zero and constant G_0 over this range of beamwidth and zero otherwise. Thus the fading spectrum

$$S(f) = \frac{\alpha G_0}{2\pi\sqrt{f_m^2-f^2}} \tag{18}$$

will be in range of $f_m\cos(\eta+\frac{\beta_b}{2})$ and $f_m\cos(\eta-\frac{\beta_b}{2})$ and zero elsewhere. The Doppler frequency shift $f_d = f_m\cos(\eta)$ at the DSN station will be in the middle of this spectrum. For high gain antennas such as the ones used in the DSN, this fading signal will produce a narrow Doppler spread and thus fairly slow signal variations are expected in the fading process.

Rather than using Jake's model, in [10] it is proved that for a high gain antenna, the fading process power spectral density can be modeled by a Gaussian shaped PSD. Therefore, from here onwards we use a Gaussian PSD in all our simulations.

Presently we don't have an accurate estimate of the Doppler spread, which depends on the DSN high gain antenna and its beamwidth, the farthest distance of regions on the surface of the Moon near south pole to the lander/rover where the transmitted waves reflect, the height of transmit antenna from the surface of the Moon, the lander/rover antenna beamwidth, and its elevation angle. So with very rough estimate we expect very low Doppler spread. In our simulations we assumed Doppler spreads of 10 Hz. The Doppler spectrum is shown in Figure 6 with 10 Hz standard deviation. In the Figure the Doppler spectrum is shifted by f_d to zero Hz.

To generate the fading process, we pass a complex white Gaussian noise process through a filter with transfer function $H(f) = \sqrt{S(f)}$, where $S(f)$ is the power spectral density of the diffuse process. To generate the Rician process, a constant can be added to this process to represent the LoS ray. The envelope of the resulting process has a Rician probability density function. Note that the overall spectrum is now a shifted version of $S(f)$ by the Doppler frequency shift f_d of the LoS ray and placing a delta function at f_d. This shift can be much larger than the Doppler spread as seen in [10]. This is the fading model that we have used in this paper.

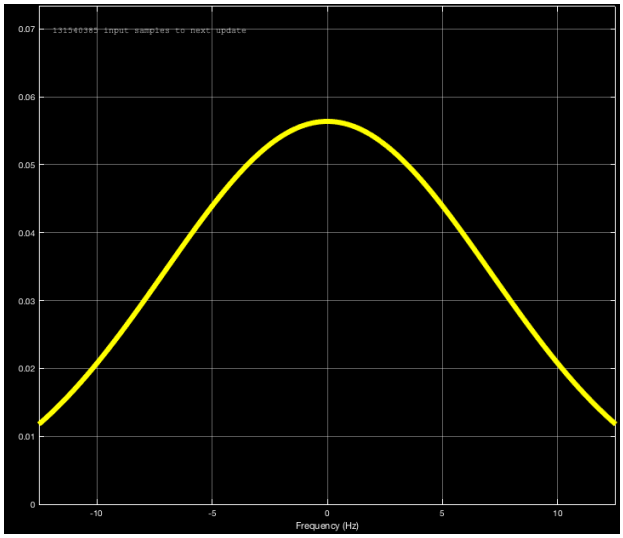

Figure 6. Gaussian shape Doppler spectrum with standard deviation of 10 Hz.

4. Performance of Uncoded BPSK in Presence of Fading with Phase Error

In this paper we consider a phase locked loop (PLL) with smart frequency sweeping to track Doppler frequency, Doppler rate, and carrier phase in the presence of a fading signal by tracking the residual carrier as a component of the received signal. Assume the average received residual carrier power over noise power spectral density is $\frac{\bar{P}_c}{N_o}$. Let B_L be the loop bandwidth of the PLL. As discussed, assuming the fading process has fairly slow variation, the instantaneous loop SNR given fading envelope ρ is approximately $\frac{\rho^2 \bar{P}_c}{N_o B_L}$. Assuming both the fading amplitude ρ and phase error ϕ are constant during a bit time interval, then the probability density function of phase error ϕ given the amplitude of fade ρ can be modeled as a Tikhonov distribution.

$$p(\phi|\rho) = \frac{e^{\frac{\rho^2 \bar{P}_c}{N_o B_L} \cos\phi}}{2\pi I_0(\frac{\rho^2 \bar{P}_c}{N_o B_L})} \tag{19}$$

The conditional bit error probability is

$$P_b(\rho, \phi) = Q(\sqrt{2\frac{\bar{E}_b}{N_o}\rho \cos\phi}) \tag{20}$$

Then the bit error probability can be calculated as

$$P_b = \int_{\rho=0}^{\infty} \int_{\phi=-\pi}^{\pi} P_b(\rho, \phi) p(\phi|\rho) p(\rho) d\phi d\rho \tag{21}$$

Using the above equation, the bit error rate P_b performance of BPSK versus the average received total power-to-noise spectral density $\frac{P_t}{N_o}$ is shown in Fig. 7. Here it is assumed that the modulation index β=60 degrees, and the loop bandwidth of the PLL is 50 Hz. Comparing the performance in this figure for the fading case with the performance when there is perfect phase tracking, we observe that the degradation due to the phase error is very small for a modulation index of 60 degrees and loop bandwidth of 50 Hz.

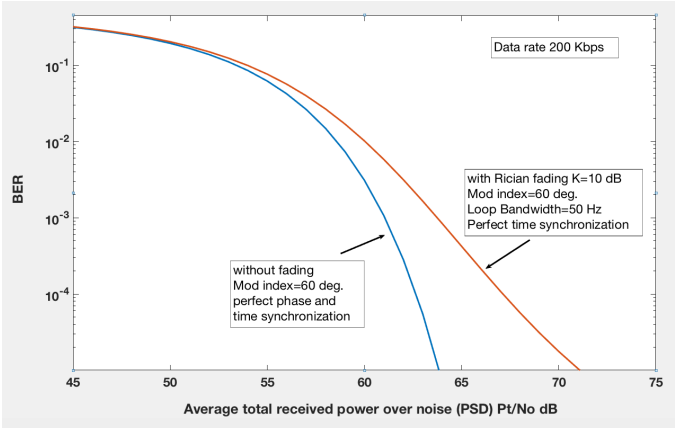

Figure 7. Analytical results for BER performance.

It is also useful to compute the variance of the phase error in multipath fading. Since the mean of the phase error ϕ is zero, then the variance of ϕ can be obtained as

$$\sigma_\phi^2 = \int_{\rho=0}^{\infty} \int_{\phi=-\pi}^{\pi} \phi^2 p(\phi|\rho) p(\rho) d\phi d\rho \tag{22}$$

5. Frequency Acquisition and Tracking using PLL with Smart Frequency Sweeping

The residual carrier can be tracked by a receiver with a phase locked loop (PLL) using a smart frequency sweeping algorithm. We use a complex signal representation for simplicity. The system block diagram at the receiver is shown in Fig. 8. In this figure the bandwidth of the low-pass filter (LPF) is slightly larger than the maximum expected frequency, which is 11.5 KHz. This LPF also reduces the interference due to data modulation on the subcarrier signal. The block diagram of the phase locked loop (PLL) is shown in Fig. 9. The new frequency sweeping algorithm is a modified version of a smart frequency sweeping method described in [11]. The new smart frequency sweeping algorithm is shown in Fig. 10. The signal P (taking values between 0 and 1 in the absence of noise and fading) is the output of the frequency lock detector in Fig. 15. Note that we already normalized the average power of fading to unity. The signal P is obtained by either integrating M samples after the mixer during each frequency interval or equivalently using a low pass filter (LPF). The parameter M or equivalently the bandwidth of the LPF should be chosen to maintain the lock stability. In contrast to the straightforward static and memoryless sweeping approach [7] and [8] that uses constant frequency step size and marches from a minimum frequency to a maximum frequency and repeats, we consider a more sophisticated but realizable algorithm that has the following characteristics: It uses multiple thresholds and changes the frequency step size when the signal P is greater than a threshold. In Fig. 10, the data flow illustrates the dynamic sweeping circuit with multiple thresholds and frequency step sizes. The signal can be acquired within seconds, and the frequency tracking error after acquisition is small compared to the loop bandwidth. The frequency acquisition algorithm that controls the frequency sweep requires the range of frequency sweep to be defined through a start frequency f_1, a final frequency f_2, and a frequency step size f_{step1} and a frequency step size f_{step2} to increment the frequency.

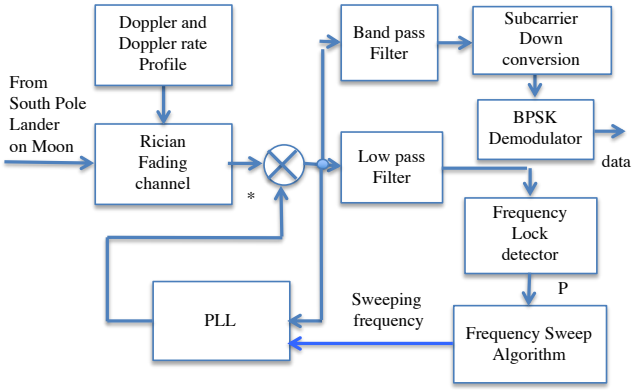

Figure 8. Receiver system block diagram with PLL.

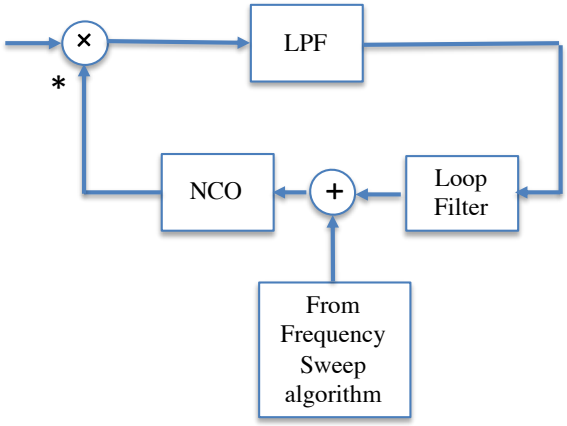

Figure 9. PLL with frequency sweeping.

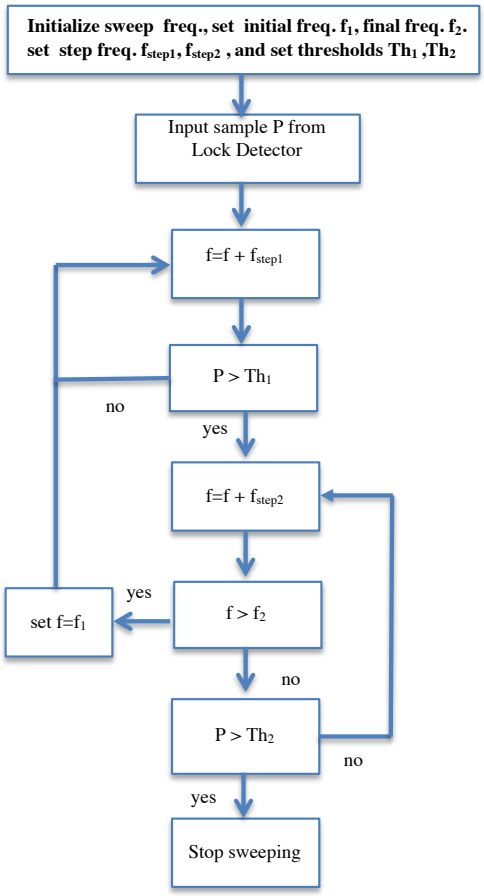

Figure 10. Frequency sweeping algorithm.

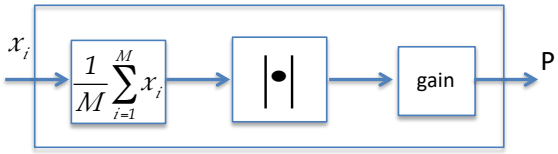

Figure 11. Lock detector.

6. A SETUP FOR SYSTEM SIMULATION

Acquisition and tracking performances are obtained using MATLAB Simulink models. The system Simulink model is shown in Fig. 12. Signals have complex representations. The frequency sweeping circuits and the lock detector are also shown in Fig. 12. The circuit for the phase locked loop (PLL) is shown in Fig. 13. The loop filter circuit with loop parameters is shown in Fig.14. The Simulink model for the lock detector and fading amplitude estimation is shown in Fig.15. The fading amplitude estimation which represents channel state information (CSI) is required for soft input channel decoders. The estimated fading amplitude also can be used to compensate for the variations of lock detector threshold output P by adjusting the gains in the lock detector. The Simulink model for the frequency sweeping algorithm is shown in Fig.16. The switches are shown by Threshold1 and Threshold2. The threshold values and frequency step size values depends to the minimum operating received carrier power to noise PSD, sampling frequency, and fading parameters and should be adjusted. For modulation index of β degrees (here we assume $\beta = 60$ degrees), the received carrier power to noise PSD is $\frac{P_c}{N_o} = \frac{P_t}{N_o}\cos^2(\beta)$ where $\frac{P_t}{N_o}$ is the total received power over noise PSD. For $\frac{P_t}{N_o}$ of 54.25 dB or equivalently $\frac{P_c}{N_o}$ of 48.25 dB, the threshold (TH1) in the switch Threshold1 is set to 0.3. The threshold (TH2) in the switch Threshold2 is set to 0.8. The initial frequency in the delay circuit is set to -15 KHz. The switch Threshold1 first selects a frequency step of 0.8 Hz per sample. When the signal P from the lock detector to the switch Threshold1 exceeds the threshold TH1 of 0.3, the frequency step size is reduced to 0.05 Hz per sample. The PLL with the smart frequency sweeping acquires and tracks Doppler frequencies in the range of -11.5 KHz to +11.5 KHz in the presence of multipath fading. In the following simulations we assumed that the current Doppler frequency is 1000 Hz and the Doppler rate is 0.735 Hz/sec. The starting frequency f_1 in the sweeping algorithm is assumed to be at 800 Hz rather than -15 kHz to get the simulation results faster in time. We assumed a loop bandwidth of 50 Hz, but a smaller loop bandwidth could be used such as 20 Hz. The lock detection signal P during frequency acquisition and tracking is shown in Fig. 17. The acquisition time depends on the starting frequency f_1 and the current Doppler frequency to be acquired. For the example in Fig. 17 the acquisition time is 0.17 seconds. Frequency tracking error after acquisition and tracking is shown in Fig. 18. The measured standard deviation of frequency error after acquisition is 18.8 Hz using a loop bandwidth of 50 Hz. The true Doppler and the PLL-estimated Doppler are shown in Fig. 19. As it can be seen in the figure, the PLL nicely tracks the initial Doppler

with Doppler rate of 0.735 Hz/sec. In this example the received residual carrier power-to-noise ratio is 48.25 dB. In this example Doppler spread of 10 Hz is assumed. The integrator in the lock detector can average out the variation in the fading if the integration time is large, however large integration time produces large delay which is not desirable, for the current setup using 20000-sample integration, still fluctuations in the threshold P are observed. In such case, the integration time in the lock detector is not enough to average out the fading amplitude. So accurate estimation of the fading amplitude is required to compensate the fading variation in the lock detector. This is subject of our future investigation. However in this example the lock detector worked without fading amplitude compensation. In absence of fading and noise the value P after Doppler frequency acquisition with normalizations (gains) that have been used in the block should settle to 1. For fading case since the value of P at the output of lock detector fluctuates with fading, in the frequency sweeping we reduced threshold (TH2) to 0.8 rather than using 1. In Fig. 20 the output of fading amplitude estimation (CSI) in Simulink model for lock detector was measured both in presence of noise and without noise. These measurements have been performed by duplication of all system components in Fig. 12 connected to the output of AWGN channel block. The input to the duplicated version then was connected to the input of AWGN channel block in Fig. 12 to measure fading amplitude estimation (CSI) in absence of noise.

The Simulink model for the modulator is shown in Fig. 21 for a modulation index of 60 degrees. This means that 1/4 of the total power is assigned to the residual carrier and 3/4 to the data. The data rate for uncoded system is assumed to be R=200 Kbps, the sampling rate is F_s=32 Msps. Thus each BPSK symbol has 160 samples. The square wave subcarrier at 400 KHz is also shown in the figure. For uncoded BPSK modulation, the received bit signal-to-noise ratio can be computed as $\frac{E_b}{N_o} = \frac{P_t}{N_o}\sin^2(\beta)\frac{1}{R}$. So for R=200 Kbps, $\frac{P_t}{N_o}$=54.25 dB, the corresponding $\frac{E_b}{N_o}$=0 dB. The Simulink model for the demodulator is shown in Fig. 22. The BPSK demodulator can provide both hard decision output or soft decision output. For soft decision output, estimates of the fading amplitudes and the variance of the noise should both be provided to the demodulator to generate log-likelihood ratios for the soft input decoder. In this paper we only considered a BPSK demodulator with hard decision output to be used for the coded system. The received BPSK signal constellation after matched filtering is shown in Fig. 23. As can be seen in the figure, the BPSK constellation shows a small phase rotation due to residual phase error at the time. However, the constellation had no rotation in time which shows that the PLL already acquired the Doppler and Doppler rate. We obtained the BER performance of the uncoded system in Fig. 12. The errors were measured after acquisition of Doppler (when the frequency sweeping algorithm stopped). The simulation results are shown in Fig. 25 and compared with the analytical results in Fig. 7. These results are in fairly good agreement. The coded system is shown in Fig. 24. We used a rate-1/2 standard CCSDS low-density parity-check (LDPC) code with information block size of 1024 bits [12]. We modeled the combination of an ideal interleaver, the uncoded system in Fig. 12, and the deinterleaver, as a binary symmetric channel (BSC) with transition probability p. The main objective of channel interleaver is to allow the consecutive faded symbols at decoder input to be spread as far as possible by deinterleaving. The ideal interleaver can be a long interleaver that makes a correlated fading channel appear memoryless at the decoder. In practice the interleaver can be implemented as a $D \times S$ block interleaver where D is the interleaver depth and it is related to the maximum fade duration. The fade duration related to the coherence time or inversely related to the Doppler spread. The parameter S is the interleaver span and it is related to the block size of a channel code. The transition probability p in the equivalent BSC channel is set equal to the BER simulation or analytical results in the uncoded system in Fig. 25 for each received total power-to-noise PSD ($\frac{P_t}{N_o}$). In the uncoded system we used Rician fading with Rician parameter K=10 dB and Doppler spread of 10 Hz while PLL was tracking the Doppler and phase. The measurements were performed after Doppler acquisition when the frequency sweeping algorithm has stopped sweeping. Then we performed a simulation of the standard rate-1/2 LDPC code with input block of 1024 bits using a belief propagation LDPC decoder over this equivalent BSC channel model. The simulation results are also shown in Fig. 25 for both bit error rate (BER) and frame error rate (FER).

7. CONCLUSIONS

In this paper we designed and analyzed an end-to-end communication system between a lander/rover on the surface of the lunar South Pole and an Earth station. The acquisition and tracking system is discussed in detail. To communicate to and from the lander/rover on the lunar South Pole, low and/or medium directional antennas onboard the lander/rover will have to be pointed at low elevation angles between 2 to 10 degrees, thus causing multipath fading effects due to reflection of a portion of the transmitted electromagnetic waves from the surface of the Moon. To design and analyze such a communication system, and in particular the acquisition and tracking system, in the presence of multipath fading, first we modeled the fading channel based on existing and simulated data. In addition to multipath fading, the channel also introduces Doppler frequency up to 11.5 KHz, and Doppler rate up to 0.735 Hz/sec. For coherent reception the Doppler frequency, which is time varying, is acquired and the incoming carrier phase, which includes the fading phase, is tracked in the presence of multipath fading. For this communication system, in addition to estimating the received carrier phase, the amplitude of the fading signal is estimated, in particular to be used in the lock detector and the channel decoder. In addition to acquisition and tracking, we considered a simple modulation/coding scheme. We designed phase locked loops and frequency sweeping schemes robust to the attenuations due to the fading. After designing various components of the communication system, we used Simulink models to obtain the end-to-end performance of the communication link. Based on the available data, the fading channel can be accurately modeled as a Rician fading channel with Rician parameter of 10 dB, and Doppler spread is assumed to be 10 Hz. Analytical and simulation results are provided for uncoded case. For the coded system with ideal interleaving we used the uncoded results and simulated the rate-1/2 standard LDPC code with a hard decision input LDPC decoder. More results for the coded system are the subject of our future research.

ACKNOWLEDGMENTS

This work was carried out at the Jet Propulsion Laboratory, California Institute of Technology, under contract with the National Aeronautics and Space Administration. We would like thank Charles H. Lee of the Jet Propulsion Laboratory, California Institute of Technology for providing Figures 3

and 4 for Doppler profile in this paper. We would like also to thank Sam Dolinar of the Jet Propulsion Laboratory, California Institute of Technology, for his valuable comments.

REFERENCES

[1] John G. Proakis, Digital Communications (3rd ed.), McGraw-Hill Book Co. Singapore, pp. 767-768, 1995.

[2] Bernard Sklar, "Rayleigh Fading Channels in Mobile Digital Communication Systems Part I: Characterization". IEEE Communications Magazine, 35 (7), 90-100, July 1997.

[3] T. S. Rappaport, Wireless Communications: Principles and Practice (2nd ed.), Prentice Hall PTR, December 31, 2001.

[4] R. H. Clarke, "A Statistical Theory of Mobile Radio Reception", Bell System Technical Journal, 47 (6), 957-1000, July-August 1968.

[5] William C. Jakes, Microwave Mobile Communications, John Wiley and Sons Inc, New York, February 1, 1975.

[6] P. Dent, G. E. Bottomley and T. Croft, "Jakes Fading Model Revisited". Electronics Letters. 29 (13), 1162-1163, 24 June 1993.

[7] C. D. Edwards, T. C. Jedrey, E. Schwartzbaum, A. S. Devereaux, R. De-Paula, M. Dapore, and T. W. Fischer, "The Electra proximity link payload for Mars relay telecommunications and navigation, IAC-03-Q.3.A06," in International Astronautical Congress 2003 , Sep.-Oct. 2003.

[8] "Autonomous Software-Defined Radio Receivers for Deep Space Applications," Jon Hamkins, Marvin K. Simon, Joseph H. Yuen (Series Editor),ISBN: 978-0-470-08212-6, Oct 2006, John Wiley and Sons.

[9] S. O. Rice, "Statistical properties of a sine wave plus random noise," Bell System Technical Journal, vol. 27, no. 1, pp. 109-157, 1948.

[10] M. Sanchez Net, "Analysis of the Fading Channel in the Downlink Between the Lunar South Pole and the Deep Space Network," Interplanetary Network Progress Report, vol. 42-215, 2018.

[11] K. Cheung, D. Divsalar, S. Bryant, "Two-Way Ranging and Doppler for Multiple Orbiting Spacecraft at Mars," IEEE Aerospace Conference 2018, Big Sky, Montana, March, 2018.

[12] Low density parity check codes for use in near-earth and deep space. Orange book, Washington, DC, USA, Sep. 2007, CCSDS standard, Issue No. 2.

BIOGRAPHY

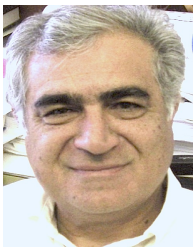

Dariush Divsalar *received the Ph.D. degree in electrical engineering from UCLA, in 1978. Since then, he has been with the Jet Propulsion Laboratory (JPL), California Institute of Technology (Caltech), Pasadena, where he is a Fellow. At JPL, he has been involved with developing state-of-the-art technology for advanced deep-space communications systems and future NASA space exploration. Since 1986, he has taught graduate courses in communications and coding at UCLA and Caltech. He has published more than 250 papers, coauthored a book entitled An Introduction to Trellis Coded Modulation with Applications, contributed to three other books, and holds 22 U.S. patents. Dr. Divsalar was a co-recipient of the 1986 paper award of the IEEE Transactions on Vehicular Technology. He was also a co-recipient of the joint paper award of the IEEE Information Theory and IEEE Communication Theory societies in 2008. The IEEE Communication Society has selected one of his papers for inclusion in a book entitled The Best of the Best: Fifty Years of Communications and Networking Research, containing the best 56 key research papers ever published in the Society's 50-year history. He has received over 50 NASA Tech Brief awards and a NASA Exceptional Engineering Achievement Medal in 1996. He served as an Editor for the IEEE Transactions on communications from 1989 to 1996.*

Marc Sanchez Net *Marc Sanchez Net is a telecommunications engineer in the Communication Architectures and Research Section at JPL. His research interests include delay tolerant networking and its impact on distributed applications such as computational task sharing, spacecraft constellation management, as well as design of space communication systems in challenged environments such as the surface of the Moon. Marc received his PhD in 2017 from MIT, and also holds degrees in both telecommunications engineering and industrial engineering from Universitat Politecnica de Catalunya, Barcelona.*

Kar-Ming Cheung *is a Principal Engineer and Technical Group Supervisor in the Communication Architectures and Research Section (332) at JPL. His group supports design and specification of future deep-space and near-Earth communication systems and architectures. Kar-Ming Cheung received NASA's Exceptional Service Medal for his work on Galileo's onboard image compression scheme. He has authored or co-authored 30+ journal papers and conference papers in the areas of error-correction coding, data compression, image processing, and telecom system operations. Since 1987 he has been with JPL where he is involved in research, development, production, operation, and management of advanced channel coding, source coding, synchronization, image restoration, and communication analysis schemes. He got his B.S.E.E. degree from the University of Michigan, Ann Arbor in 1984, his M.S. degree and Ph.D. degree from California Institute of Technology in 1985 and 1987 respectively.*

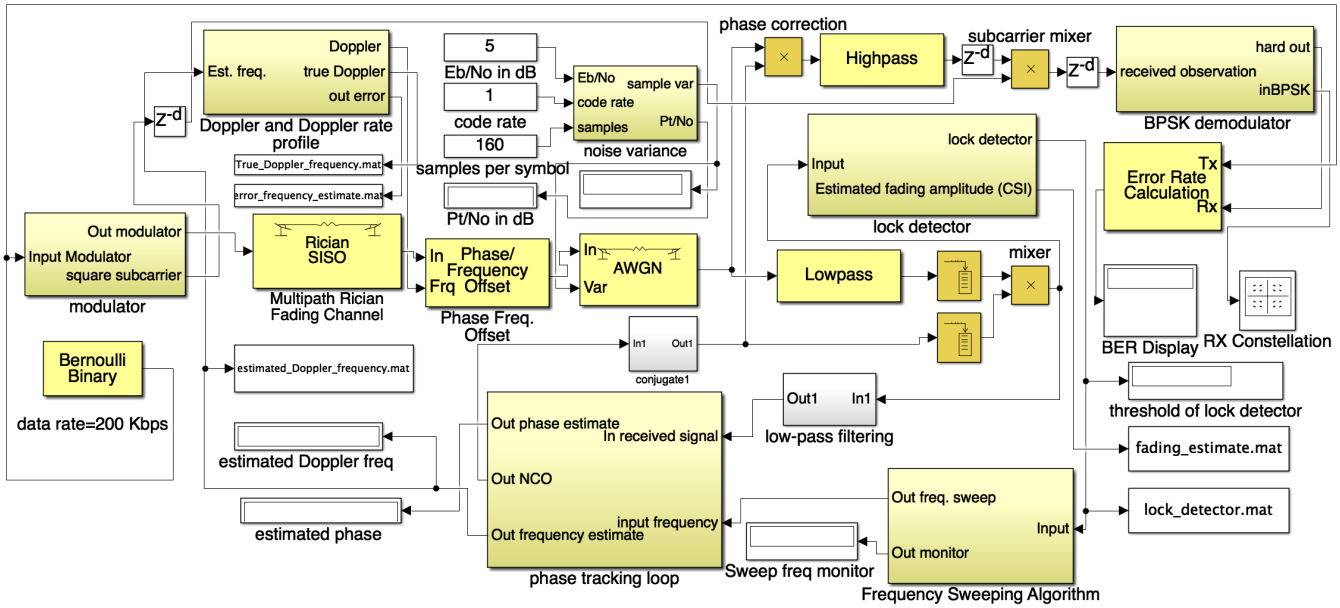

Figure 12. Simulink model for uncoded system.

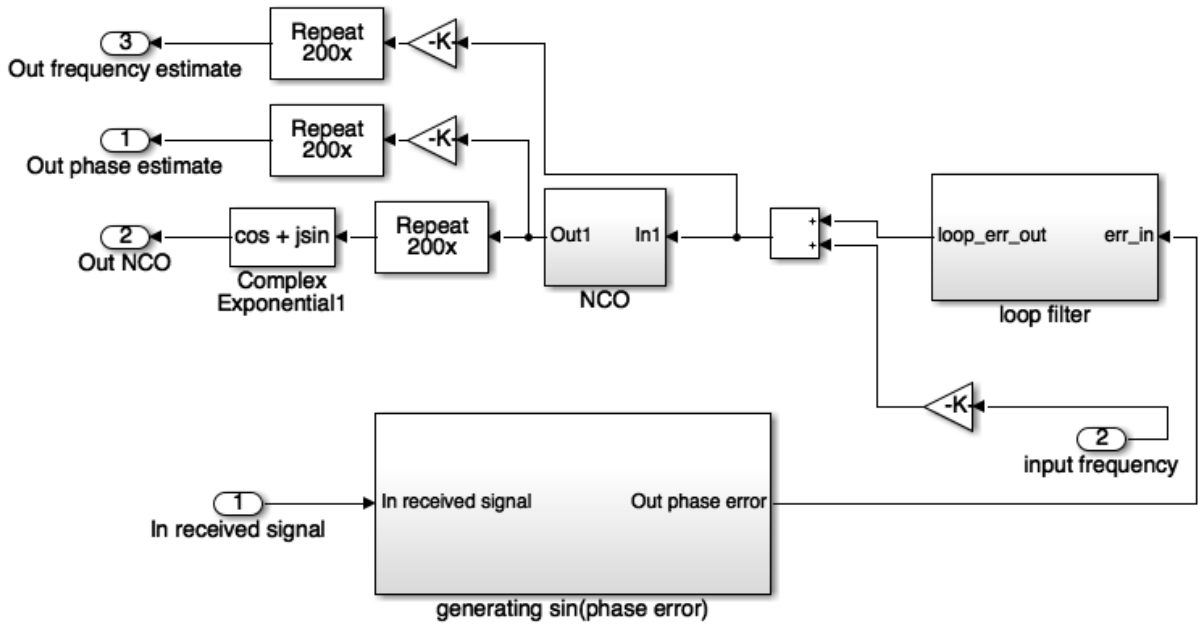

Figure 13. Simulink PLL model.

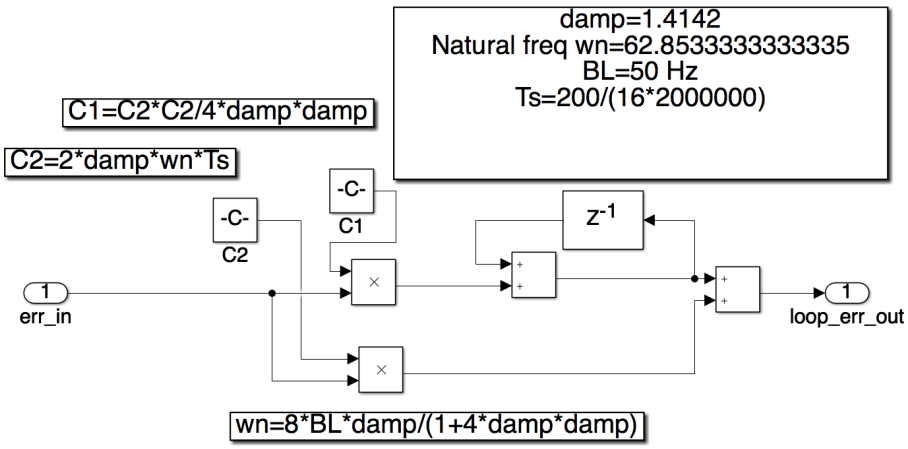

Figure 14. Simulink Loop Filter model

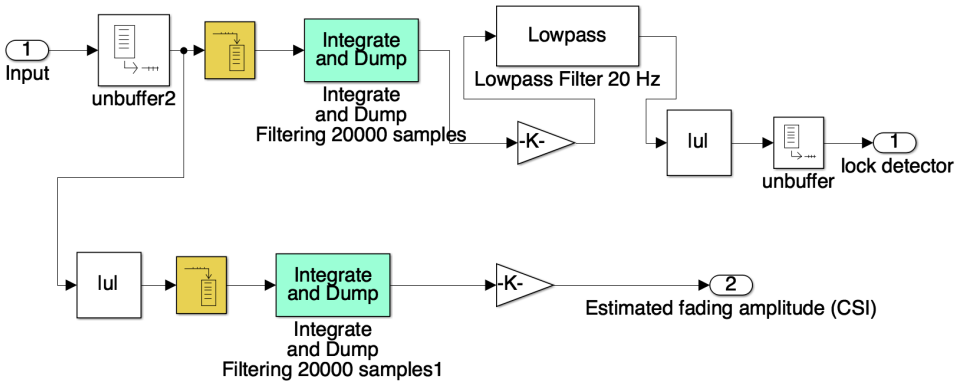

Figure 15. Simulink Lock Detector and Channel State Information (CSI) model

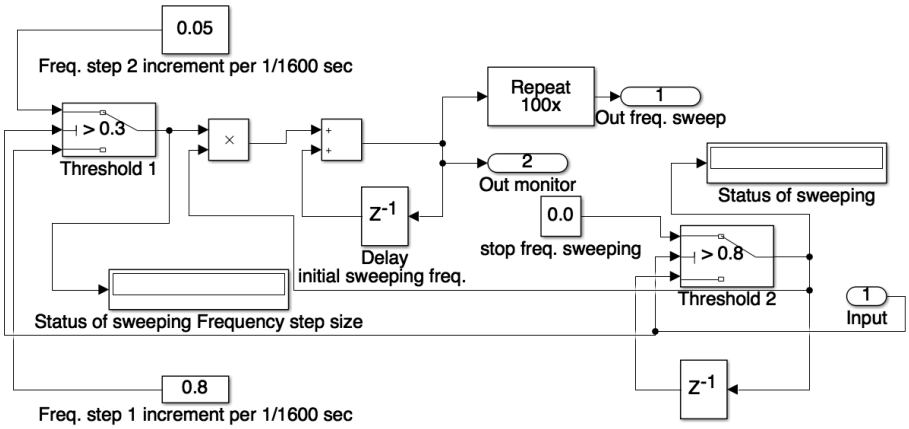

Figure 16. Simulink Frequency sweep model

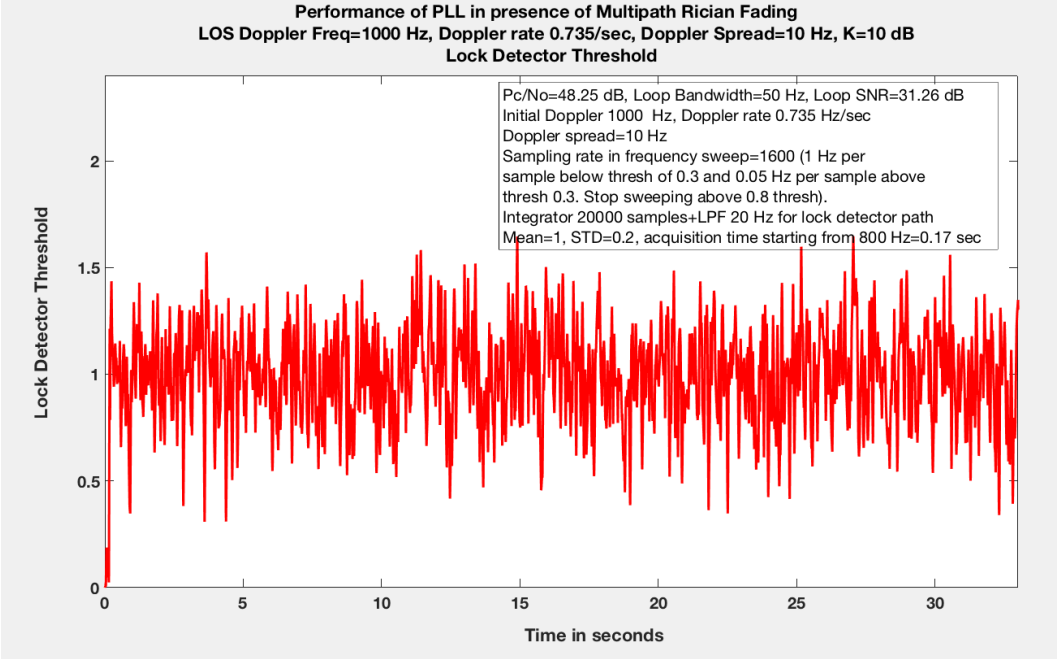

Figure 17. Lock detector output P

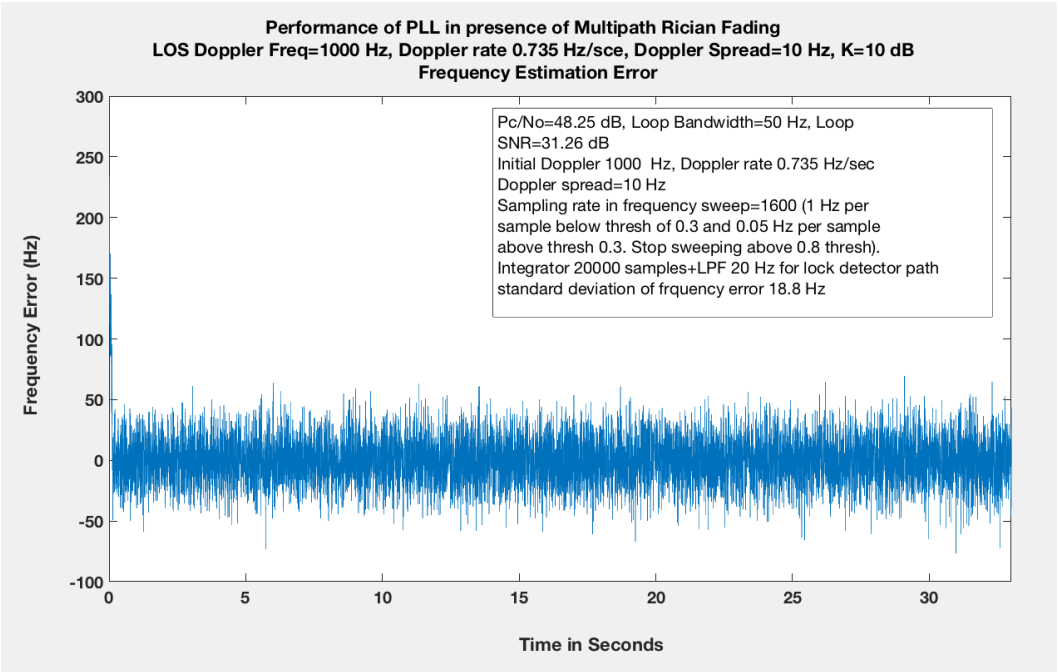

Figure 18. Frequency error.

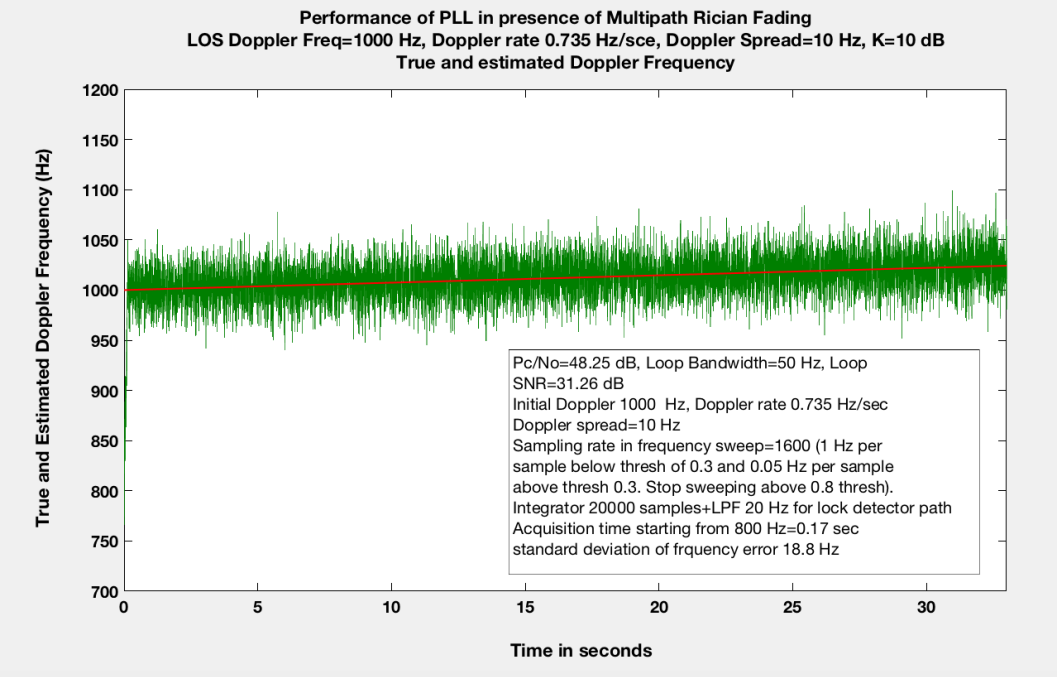

Figure 19. True and estimated Doppler frequency.

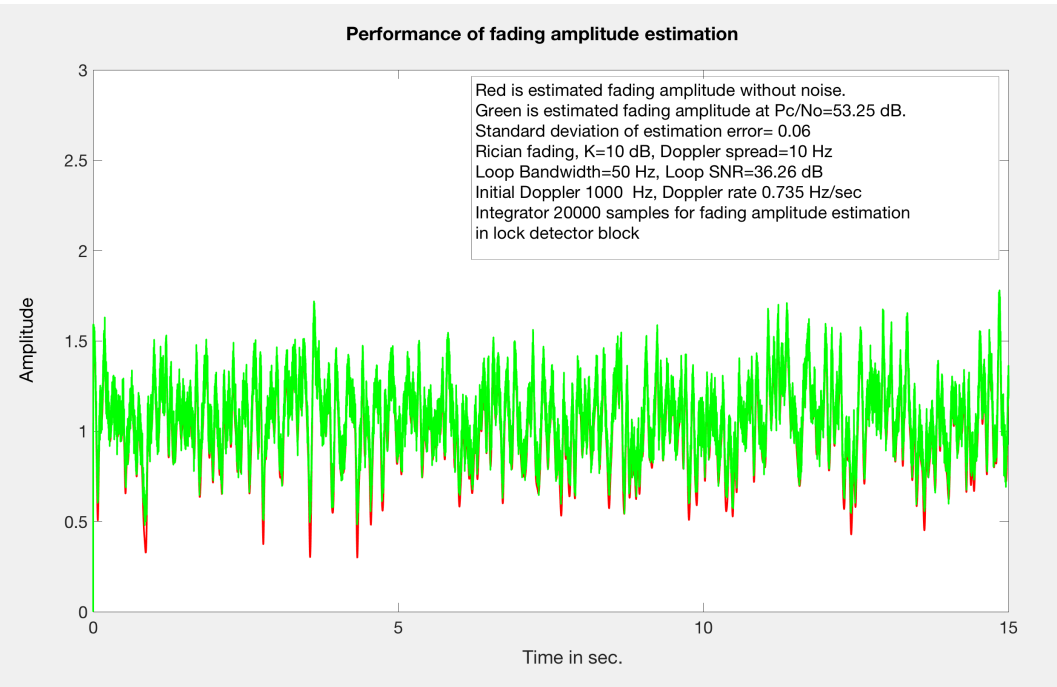

Figure 20. Fading amplitude estimation with and without noise.

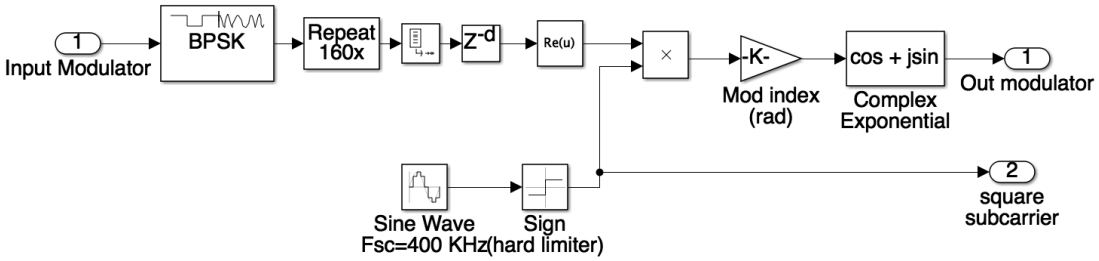

Figure 21. Simulink modulator model

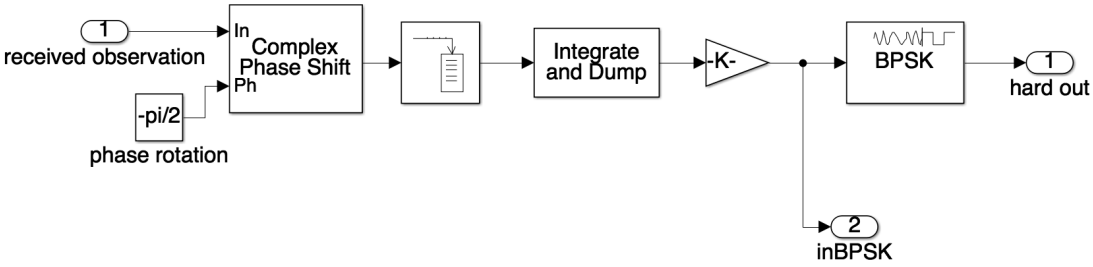

Figure 22. Simulink demodulator model

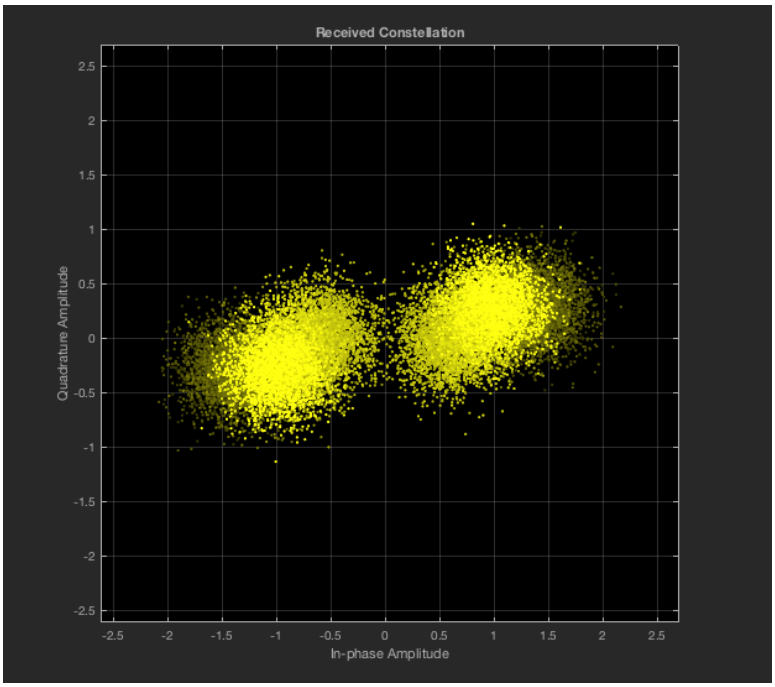

Figure 23. Received BPSK signal after matched filtering after Doppler acquisition

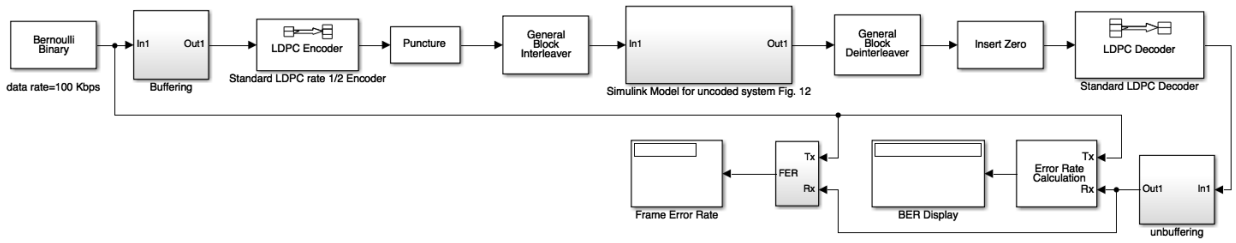

Figure 24. Simulink coded system model

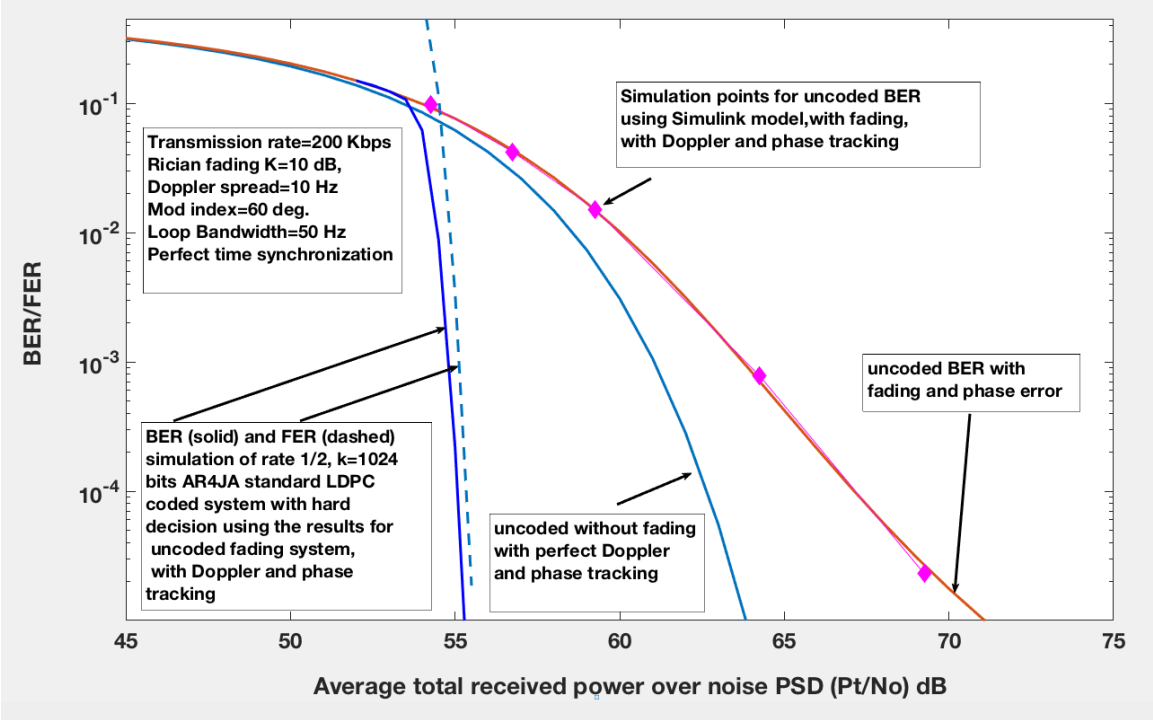

Figure 25. Simulation results for BER/FER of rate 1/2 standard LDPC code with hard decision input decoder.